Available online at www.sciencedirect.com

ScienceDirect

Journal of Otology 11 (2016) 127–133

www.journals.elsevier.com/journal-of-otology/

Label-free visualization of cholesteatoma in the mastoid and tympanic membrane using CARS microscopy ☆

Jing Zou [a,b,*], Antti Isomäki [d], Timo Hirvonen [c], Antti Aarnisalo [c], Jussi Jero [c], Ilmari Pyykkö [b]

[a] *Department of Otolaryngology-Head and Neck Surgery, Center for Otolaryngology-Head & Neck Surgery of Chinese PLA, Changhai Hospital, Second Military Medical University, Shanghai, China*

[b] *Hearing and Balance Research Unit, Field of Oto-laryngology, School of Medicine, University of Tampere, Tampere, Finland*

[c] *Department of Otorhinolaryngology-Head and Neck Surgery, Helsinki University Central Hospital, Helsinki, Finland*

[d] *Biomedicum Imaging Unit, Faculty of Medicine, University of Helsinki, Helsinki, Finland*

Received 18 August 2016; revised 2 September 2016; accepted 6 September 2016

Abstract

Objective: The present study aimed to evaluate the possibility of using coherent anti-Stokes Raman spectroscopy (CARS) microscopy to determine the specific molecular morphology of cholesteatoma by detecting the natural vibrational contrast of the chemical bonds without any staining.

Materials and methods: Specimens from the mastoid and tympanic membrane with and without cholesteatoma were analyzed using CARS microscopy, two-photon excited fluorescence (TPEF) microscopy, and the second harmonic generation (SHG) microscopy.

Results: In cholesteatoma tissues from the mastoid, a strong resonant signal at 2845 cm^{-1} was observed by CARS, which indicated the detection of the CH_2 hydro-carbon lipid bonds that do not generate visible signals at 2940 cm^{-1} suggestive of CH_3 bonds in amino acids. A strong resonant signal at 2940 cm^{-1} appeared in an area of the same specimen, which also generated abundant signals by TPEF and SHG microscopy at 817 nm, which was suggestive of collagen. In the tympanic membrane specimen with cholesteatoma, a strong resonant signal with corrugated morphology was detected, which indicated the presence of lipids. A strong signal was detected in the tympanic membrane with chronic otitis media using TPEF/SHG at 817 nm, which indicated collagen enrichment. The CARS and TPEF/SHG images were in accordance with the histology results.

Conclusion: These results suggest the need to develop a novel CARS microendoscope that can be used in combination with TPEF/SHG to distinguish cholesteatoma from inflammatory tissues.

Keywords: Cholesteatoma; Imaging; Label-free; Raman spectroscopy; High resolution

1. Introduction

Cholesteatoma is a benign, gradually expanding destructive cystic epithelial lesion of the temporal bone that is generated from keratinizing stratified squamous epithelium (Semaan and Megerian, 2006). Surgical removal of the pathological tissue is the only effective therapy for cholesteatoma, but some cases of cholesteatoma can recur after this procedure (Tomlin et al., 2013; Neudert et al., 2014). Indeed, the rate of residual

☆ This study was supported by grants from Ministry of Science and Technology of China, China-EU collaborative project (Grant No. 0S2014GR0137).

* Corresponding author. Department of Otolaryngology-Head and Neck Surgery, Changhai Hospital, Second Military Medical University, Changhai Road #168, Shanghai 200433, China.

E-mail addresses: Jing.Zou@uta.fi, zoujinghb@hotmail.com (J. Zou).

Peer review under responsibility of PLA General Hospital Department of Otolaryngology Head and Neck Surgery.

http://dx.doi.org/10.1016/j.joto.2016.09.001

cholesteatoma following surgery can reach as high as 35%, and surgery is the major contribution to recurrence in the clinic (Wilson et al., 2013). Even the application of endoscope during surgery in combination with operating microscope only provides an incremental benefit for prevention of residual cholesteatoma (James et al., 2016). Our hypothesis is that the conventional endoscope has a limitation in detecting focal cholesteatoma due to its lower spatial resolution and poorer depth sensation than the operating microscope. Therefore, there is a need to improve the visualization by developing a novel endoscopic approach that is capable of detecting the specific chemical structures within the cholesteatoma to assure a clear surgical margin during surgery. This potential novel endoscope may also be useful to predict which retraction pocket on the tympanic membrane will develop into cholesteatoma and guide the treatment strategy in the clinic.

Raman spectroscopy is a powerful tool capable of generating a characteristic signature of the sample material and operates by detecting energy associated with the molecular bond vibrations. The process in which the incident photons scatter inelastically upon interaction with matter is also known as Raman scattering (Wachsmann-Hogiu et al., 2009). Pandey et al. reported that Raman spectroscopy is capable of discerning the molecular pathology of differential proliferative middle ear lesions and may aid in the assessment of pathological borders to improve surgical outcomes in cases of middle ear disease (Pandey et al., 2015). However, the Raman spectroscopy signal is faint and insufficient for clinical application during surgery. High-resolution coherent anti-Stokes Raman spectroscopy (CARS) is an advanced molecular imaging technique that has recently been applied to label-free imaging of cells and tissues using the natural vibrational contrast and has significantly boosted and enhanced Raman signal levels (Pezacki et al., 2011; Moura et al., 2016). CARS occurs when a target molecule is simultaneously irradiated by two laser beams at different frequencies, a pump beam ω_P and a Stokes beam ω_S. When the difference between the higher frequency (pump beam) and the lower frequency (Stokes beam) equals the vibrational frequency of the target bond of the molecule, a CARS signal is generated (Pezacki et al., 2011; Folick et al., 2011; Rodriguez et al., 2006).

We aimed to evaluate the feasibility of using CARS microscopy to display the specific molecular morphology of cholesteatoma and the potential of CARS to be integrated as a novel endoscope for cholesteatoma imaging in the clinic. We focused on detecting the vibrations of CH_2 bonds in the lipids accumulated in the cholesteatoma and the CH_3 bonds in the peptides of proteins that are enriched in the tissues of chronic suppurative otitis media attributed to the inflammatory infiltrations and biofilm formation, among others (Fig. 1) (Bloksgaard et al., 2012; Gu et al., 2014; Knutsson et al., 2011; Uno and Saito, 1995). Two-photon excited fluorescence (TPEF) and potentially the second harmonic generation (SHG) from fibrillar collagen structures caused by chronic inflammation was also evaluated (Knutsson et al., 2011; Uno and Saito, 1995; Jiang et al., 2011).

2. Materials and methods

2.1. Specimens

The following 4 types of specimens were collected from 3 patients undergoing middle ear surgeries at the Helsinki University Central Hospital: cholesteatoma tissues from the mastoid, the mucosa of the temporal bone air cell without visible cholesteatoma in the same mastoid that was 10 mm away from the identified cholesteatoma, the tympanic membrane with cholesteatoma on the mucosa layer, and the residual membrane near the perforation of the tympanic membrane of chronic otitis media. After surgical removal, all specimens were immediately fixed using 4% formaldehyde overnight and maintained in phosphate-buffered saline (PBS, 0.01 M, pH 7.4) until CARS microscopy and histology study. No additional procedures were added to the standard surgery when the specimens were obtained, and no personal information was exposed. The study protocol was approved by the ethics committee of the Helsinki University Central Hospital and followed the rules of the Declaration of Helsinki, which was developed by the World Medical Association and was updated at the 64th WMA General Assembly in Fortaleza, Brazil, in 2013 (WMA Declaration of Helsinki – Ethical Principles for Medical Research Involving Human Subjects, 2014).

2.2. CARS microscopy

The images were acquired with a commercial Leica TCS SP8 CARS confocal microscope (Leica Microsystems GmbH, Wetzlar, Germany), which consists of an inverted microscope equipped with an ultra-short pulsed light source (picoEmerald, APE, Berlin, Germany) that produces the two synchronous beams needed for CARS microscopy. The Stokes beam at 1064 nm was emitted from a neodymium-doped yttrium orthovanadate ($Nd:YVO_4$) laser while a tunable pump/probe beam at 780–940 nm was generated by an optical parametric oscillator (OPO). The pulse width was 5–7 ps with a repetition rate of 80 MHz corresponding to the Raman line width of 2–3 cm^{-1}. The pulses from the two sources were temporally and spatially overlapped on the focal plane of the microscope. Up to 100 mW of average power from both the pump and the Stokes source was delivered to the specimen with an identical laser intensity for each measurement. The laser generating wavelength of 817 nm was used for the CARS modality simultaneously with the Stokes beam at 1064 nm to excite the symmetric vibrational resonance of the CH_2 hydro-carbon bonds in the lipids at 2845 cm^{-1} and that of the CH_3 bonds in amino acids of the proteins at 2940 cm^{-1} (Pirhonen et al., 2016; Surmacki et al., 2013). Meanwhile, the TPEF and SHG was measured using excitation at 817 nm and broad-band detection at 380 nm – 550 nm according to the literature (Jiang et al., 2011). The detected TPEF was compared with the conventional autofluorescent microscopy measured with 488 nm excitation. The generated two-photon excited and

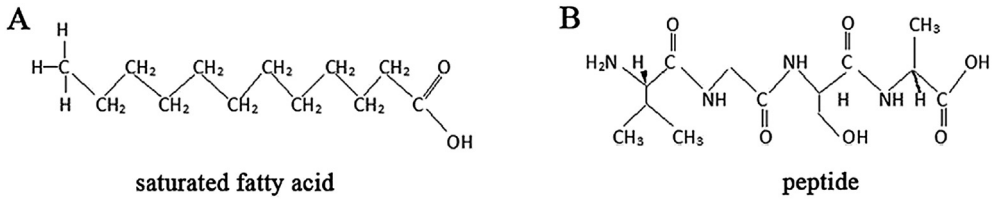

Fig. 1. Chemical structures of a saturated fatty acid and peptide. There are plenty of CH_2 bonds in the saturated fatty acid (A) and CH_3 bonds in the peptide (B).

CARS signals were detected in the epi-direction using a non-descanned photomultiplier tube (PMT) detector.

The images were acquired from formaldehyde-fixed tissues using a 25× water immersion objective (Leica HCX IR APO L 25×/0.95 W). All images were recorded using the Leica Application Suite X (LAS X) software (Leica Microsystems GmbH, Wetzlar, Germany).

2.3. Histological study

After CARS microscopy, the specimens were embedded in paraffin and sectioned at 4 μm thickness using a standard protocol. The sections were processed for hematoxylin-eosin (H & E) staining after deparaffinization by following a standard protocol. The slices were observed under a light microscope (Leica DM2000 microscope) equipped with an Olympus DP25 camera (Olympus Corporation, Tokyo, Japan).

3. Results

3.1. CARS microscopy

In the cholesteatoma tissue collected from the mastoid, a strong resonant signal occurred at 2845 cm^{-1} indicating

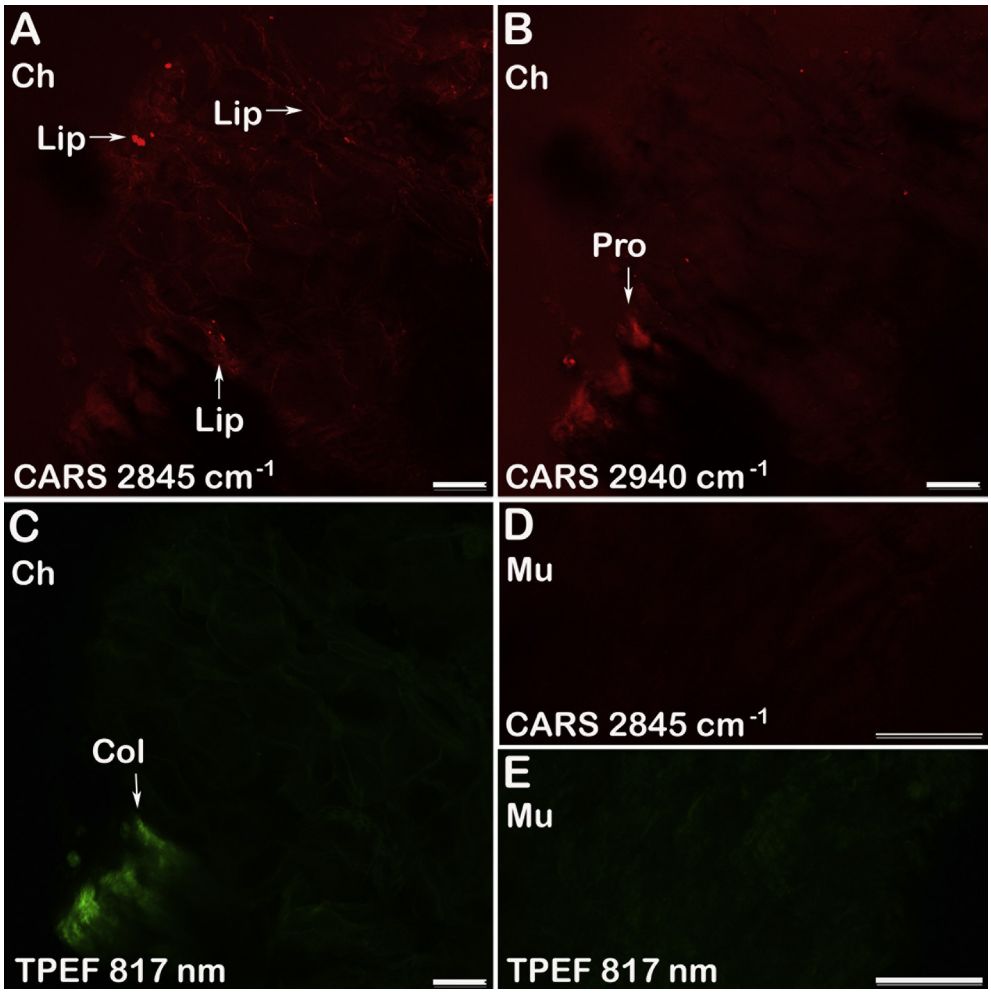

Fig. 2. Comparison of label-free CARS microscopy and SHG/TPEF of cholesteatoma tissue and mucosa of the temporal bone air cell in the mastoid. Strong resonant signals at 2845 cm^{-1} and 2940 cm^{-1} and a SHG/TPEF signal at 817 nm excitation were detected in the cholesteatoma tissue (Ch) in different areas (A–C). Weak resonant signals at 2845 cm^{-1} and a SHG/TPEF signal in the mucosa (Mu) of the temporal bone air cell in the mastoid were observed (D, E). Col: collagen; Lip: lipid; Pro: protein. Scale bar = 25 μm (A–C) and 50 μm (D, E).

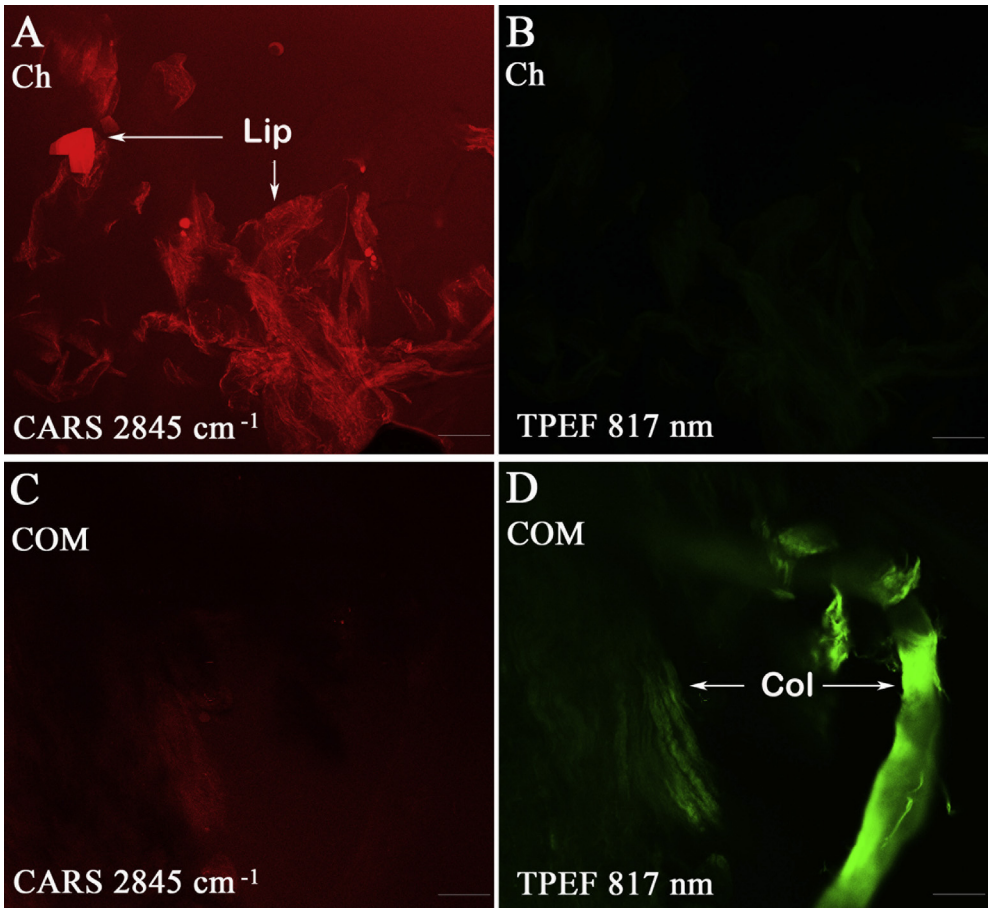

Fig. 3. Comparison of label-free CARS microscopy of the tympanic membrane with cholesteatoma on the mucosa layer and the residual membrane near the perforation of the tympanic membrane in chronic otitis media (COM). The tympanic membrane with cholesteatoma (Ch) displayed a strong resonant signal at 2845 cm^{-1} but only weak autofluorescence and no SHG excited by the 817 nm laser (A, B). The tympanic membrane of COM did not produce a resonant signal at 2845 cm^{-1} but did exhibit a strong SHG/TPEF signal (C, D). Col: collagen; Lip: lipid. Scale bar = 25 μm.

detection of the CH_2 hydro-carbon bonds of the lipids, which displayed corrugated morphology with occasional bright spots. These structures did not generate visible signals at 2940 cm^{-1}, which is thought to excite the CH_3 bonds in the amino acids of proteins. However, a strong resonant signal at 2940 cm^{-1} appeared in an area of the same specimen, which generated abundant SHG signals excited at 817 nm, suggestive of collagen. A weak signal was detected in the lipid area of the cholesteatoma tissue and the mucosa of the temporal bone air cell in the same mastoid using 817 nm excitation (Fig. 2).

In the tympanic membrane with cholesteatoma on the mucosa layer specimen, a strong resonant signal with corrugated morphology was detected at 2845 cm^{-1}, indicating the presence of CH_2 hydro-carbon bonds of the lipids. Excitation at 817 nm did not lead to emission from the same specimen. However, a strong SHG/TPEF signal was generated on the residual membrane near the perforation of the tympanic membrane of chronic otitis media using 817 nm excitation, which indicated collagen enrichment. CARS microscopy showed only a weak resonant signal at 2845 cm^{-1}, which was expected to excite lipids (Fig. 3).

The observed results were consistent in all analyzed specimens without exception.

3.2. Histology

H & E staining demonstrated the appearance of specific lipids with obvious corrugated morphology in the specimens of cholesteatoma tissue collected from the mastoid and tympanic membrane with cholesteatoma on the mucosa layer. Extensive infiltration of inflammatory cells appeared in the specimens of the mucosa of the temporal bone air cell in the mastoid and the residual membrane near the perforation of the tympanic membrane in chronic otitis media. Proliferations of connective tissue and epithelial cells were demonstrated in the specimen of residual membrane near the perforation of the tympanic membrane in chronic otitis media (Fig. 4).

4. Discussions

The present study demonstrated that CARS microscopy depicted specific images of cholesteatoma in the mastoid and tympanic membrane by exciting the symmetric vibrational

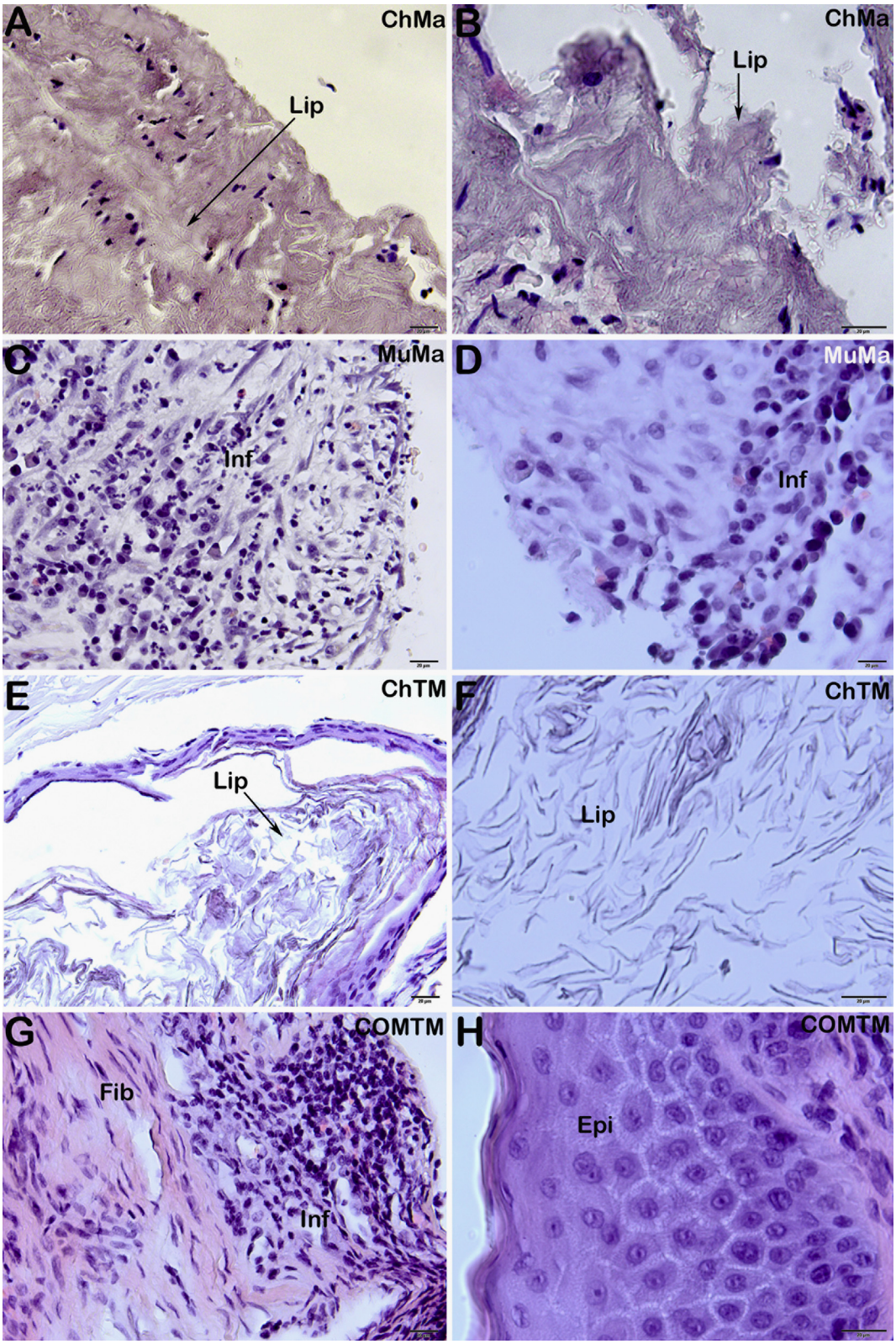

Fig. 4. H.E. staining of cholesteatoma tissue and inflammatory tissue of the temporal bone air cell in the mastoid and tympanic membrane. Lipids with obvious corrugated morphology appeared in the cholesteatoma tissues of the temporal bone air cell in the mastoid (ChMa) and tympanic membrane (ChTM) (A, B, E, and F). Infiltration of inflammatory cells were detected in the mucosa of the temporal bone air cell in the mastoid (MuMa) and the residual membrane near the perforation of the tympanic membrane in chronic otitis media (COMTM) (C, D, G, and H). There was obvious proliferation of connective tissue and epithelial cells in the tympanic membrane of chronic otitis media (G, H). Epi: epithelial cells; Fib: collagen fibers; Inf: infiltration of inflammatory cells; Lip: lipids. Scale bar = 20 μm.

resonance of the CH_2 hydro-carbon bonds in the lipids at 2845 cm^{-1} using a laser generating wavelength of 817 nm for the CARS modality simultaneously with the Stokes beam at 1064 nm. Meanwhile, the enrichment of collagen in the proliferated connective tissue of the residual tympanic membrane of chronic otitis media and the cholesteatoma in the mastoid was displayed using SHG/TPEF at 817 nm. The CARS microscopic images and SHG/TPEF images were in accordance with the histological results. The existence of collagen fiber bundles in cholesteatoma tissues has been reported, and these collagen fibers are composed of types I, II, and IV (Knutsson et al., 2011). There has been no report regarding collagen composition of the cholesteatoma in the human tympanic membrane. However, there was a report on the collagen structure of a healthy tympanic membrane during healing of a perforation and during infection in an animal model (Stenfeldt et al., 2006). In the animal model study, type II collagen was the main constituent of the lamina propria of the pars tensa. After myringotomy, collagen types I and III were found at the perforation border and around the dilated blood vessels early in the healing phase. During infection, the collagen layer was thickened and stained strongly for type II collagen. Collagen types I and III were found in the edematous connective tissue around the main collagen layer and around dilated blood vessels. Three months after perforation or infection, all 3 collagens were present in the lamina propria of the tympanic membrane (Stenfeldt et al., 2006).

These results provided evidence for the need to develop a novel CARS microendoscope that can be used in combination with a SHG/TPEF microscope to distinguish the cholesteatoma from inflammatory tissues. The potential imaging system may also help detect residuals on dural surfaces in large petrous bone cholesteatoma and epidermoid lesions during surgery. Diffusion weighted MRI (DWMRI) has been reported to be able to differentiate recurrent cholesteatoma from granulation tissue after mastoidectomy (Maheshwari and Mukherji, 2002; De Foer et al., 2008). However, it impossible to apply MRI during surgery. There is a limitation for DWMRI to detect cholesteatoma in the tympanic membrane due to its thin structure. The current laser systems are very expensive but an affordable solution could potentially be developed in the future. Some studies have reported the development of a CARS endoscope, although the system needs further improvement (Brustlein et al., 2011; Satira, 2013). It is feasible to develop a hybrid microscopic system using CARS and SHG/TPEF for clinical application in cholesteatoma.

In conclusion, the present study demonstrated that CARS microscopy is capable of visualizing the cholesteatoma in the mastoid and tympanic membrane by exciting the symmetric vibrational resonance of the CH_2 hydro-carbon bonds in the lipids and distinguishing the inflammatory mucosa from the tympanic membrane with perforation. The SHG/TPEF excited at 817 nm is effective for visualizing the existence of collagen bundles in inflammatory tissues. There is a potential to develop CARS endoscope for in vivo detection of cholesteatoma in patients.

References

Bloksgaard, M., Svane-Knudsen, V., Sorensen, J.A., Bagatolli, L., Brewer, J., 2012. Structural characterization and lipid composition of acquired cholesteatoma: a comparative study with normal skin. Otol. Neurotol. 33 (2), 177−183. http://dx.doi.org/10.1097/MAO.0b013e318241be63.

Brustlein, S., Berto, P., Hostein, R., Ferrand, P., Billaudeau, C., Marguet, D., Muir, A., Knight, J., Rigneault, H., 2011. Double-clad hollow core photonic crystal fiber for coherent Raman endoscope. Opt. Express 19 (13), 12562−12568. http://dx.doi.org/10.1364/OE.19.012562.

De Foer, B., Vercruysse, J.P., Bernaerts, A., Deckers, F., Pouillon, M., Somers, T., Casselman, J., Offeciers, E., 2008. Detection of postoperative residual cholesteatoma with non-echo-planar diffusion-weighted magnetic resonance imaging. Otol. Neurotol. 29 (4), 513−517. http://dx.doi.org/10.1097/MAO.0b013e31816c7c3b.

Folick, A., Min, W., Wang, M.C., 2011. Label-free imaging of lipid dynamics using coherent anti-stokes Raman scattering (CARS) and Stimulated Raman scattering (SRS) microscopy. Curr. Opin. Genet. Dev. 21 (5), 585−590. http://dx.doi.org/10.1016/j.gde.2011.09.003.

Gu, X., Keyoumu, Y., Long, L., Zhang, H., 2014. Detection of bacterial biofilms in different types of chronic otitis media. Eur. Arch. Otorhinolaryngol. 271 (11), 2877−2883. http://dx.doi.org/10.1007/s00405-013-2766-8.

James, A.L., Cushing, S., Papsin, B.C., 2016. Residual cholesteatoma after endoscope-guided surgery in children. Otol. Neurotol. 37 (2), 196−201. http://dx.doi.org/10.1097/MAO.0000000000000948.

Jiang, X., Zhong, J., Liu, Y., Yu, H., Zhuo, S., Chen, J., 2011. Two-photon fluorescence and second-harmonic generation imaging of collagen in human tissue based on multiphoton microscopy. Scanning 33 (1), 53−56. http://dx.doi.org/10.1002/sca.20219.

Knutsson, J., Bagger-Sjoback, D., von Unge, M., 2011. Structural tympanic membrane changes in secretory otitis media and cholesteatoma. Otol. Neurotol. 32 (4), 596−601. http://dx.doi.org/10.1097/MAO.0b013e318214ea62.

Maheshwari, S., Mukherji, S.K., 2002. Diffusion-weighted imaging for differentiating recurrent cholesteatoma from granulation tissue after mastoidectomy: case report. AJNR Am. J. Neuroradiol. 23 (5), 847−849.

Moura, C.C., Tare, R.S., Oreffo, R.O., Mahajan, S., 2016. Raman spectroscopy and coherent anti-Stokes Raman scattering imaging: prospective tools for monitoring skeletal cells and skeletal regeneration. J. R. Soc. Interface 13 (118). http://dx.doi.org/10.1098/rsif.2016.0182.

Neudert, M., Lailach, S., Lasurashvili, N., Kemper, M., Beleites, T., Zahnert, T., 2014. Cholesteatoma recidivism: comparison of three different surgical techniques. Otol. Neurotol. 35 (10), 1801−1808. http://dx.doi.org/10.1097/MAO.0000000000000484.

Pandey, R., Paidi, S.K., Kang, J.W., Spegazzini, N., Dasari, R.R., Valdez, T.A., Barman, I., 2015. Discerning the differential molecular pathology of proliferative middle ear lesions using Raman spectroscopy. Sci. Rep. 5, 13305. http://dx.doi.org/10.1038/srep13305.

Pezacki, J.P., Blake, J.A., Danielson, D.C., Kennedy, D.C., Lyn, R.K., Singaravelu, R., 2011. Chemical contrast for imaging living systems: molecular vibrations drive CARS microscopy. Nat. Chem. Biol. 7 (3), 137−145. http://dx.doi.org/10.1038/nchembio.525.

Pirhonen, J., Arola, J., Sadevirta, S., Luukkonen, P., Karppinen, S.M., Pihlajaniemi, T., Isomaki, A., Hukkanen, M., Yki-Jarvinen, H., Ikonen, E., 2016. Continuous grading of early fibrosis in NAFLD using label-free imaging: a proof-of-concept study. PLoS One 11 (1). http://dx.doi.org/10.1371/journal.pone.0147804 e0147804.

Rodriguez, L.G., Lockett, S.J., Holtom, G.R., 2006. Coherent anti-stokes Raman scattering microscopy: a biological review. Cytom. A 69 (8), 779−791. http://dx.doi.org/10.1002/cyto.a.20299.

Satira, Z.A., 2013. Theoretical investigation of material properties affecting coherent anti-stokes Raman scattering microendoscopy. Research, Rice University, Houston, Texas, USA.

Semaan, M.T., Megerian, C.A., 2006. The pathophysiology of cholesteatoma. Otolaryngol. Clin. North Am. 39 (6), 1143−1159. http://dx.doi.org/10.1016/j.otc.2006.08.003.

Stenfeldt, K., Johansson, C., Hellstrom, S., 2006. The collagen structure of the tympanic membrane: collagen types I, II, and III in the healthy tympanic

membrane, during healing of a perforation, and during infection. Arch. Otolaryngol. Head. Neck Surg. 132 (3), 293–298. http://dx.doi.org/10.1001/archotol.132.3.293.

Surmacki, J., Musial, J., Kordek, R., Abramczyk, H., 2013. Raman imaging at biological interfaces: applications in breast cancer diagnosis. Mol. Cancer 12, 48. http://dx.doi.org/10.1186/1476-4598-12-48.

Tomlin, J., Chang, D., McCutcheon, B., Harris, J., 2013. Surgical technique and recurrence in cholesteatoma: a meta-analysis. Audiol. Neurootol 18 (3), 135–142. http://dx.doi.org/10.1159/000346140.

Uno, Y., Saito, R., 1995. Bone resorption in human cholesteatoma: morphological study with scanning electron microscopy. Ann. Otol. Rhinol. Laryngol. 104 (6), 463–468.

Wachsmann-Hogiu, S., Weeks, T., Huser, T., 2009. Chemical analysis in vivo and in vitro by Raman spectroscopy–from single cells to humans. Curr. Opin. Biotechnol. 20 (1), 63–73. http://dx.doi.org/10.1016/j.copbio.2009.02.006.

Wilson, K.F., Hoggan, R.N., Shelton, C., 2013. Tympanoplasty with intact canal wall mastoidectomy for cholesteatoma: long-term surgical outcomes. Otolaryngol. Head. Neck Surg. 149 (2), 292–295. http://dx.doi.org/10.1177/0194599813489521.

WMA Declaration of Helsinki - Ethical Principles for Medical Research Involving Human Subjects, 2014. World Medical Association. http://www.wma.net/en/30publications/10policies/b3/.